Supplementary Material for On-chip, inverse-designed active wavelength division multiplexer at THz frequencies

Valerio Digiorgio[1*], Urban Senica[1], Paolo Micheletti[1], Mattias Beck[1],
Jérôme Faist[1], Giacomo Scalari[1*]

[1]Institute for Quantum Electronics, ETH Zürich, 8093 Zürich, Switzerland

* To whom correspondence should be addressed;
E-mail: vdigiorgio@phys.ethz.ch, gscalari@ethz.ch

Materials and Methods

Sample Fabrication and Mounting

The laser chips were fabricated from MBE-grown wafers of the active material, consisting of a strongly diagonal, low-threshold broadband GaAs/AlGaAs heterostructure. The fabrication process follows a planarized waveguide technique, described in Ref.[1]. Samples of a typical size of (9x10)mm^2 are cleaved. A metallic stack is deposited on the sample and on a n+ GaAs carrier substrate. The two are bonded by thermocompression wafer bonding, after which mechanical polishing and wet-etching are needed to expose the active region. The active waveguides are then defined using inductively-coupled plasma (ICP) etching, employing a Au self-aligned mask. After dry-etching, the sample is treated with a microelectronic-grade low-loss polymer, benzocyclobutene (BCB), which is spin-coated and baked as the surrounding material. Specifically, we use Cyclotene 3022-57 (BCB), with a refractive index of 1.57 and relatively low losses (3 cm^{-1}=1.3 dB/mm) at 3 THz, making it an ideal planarization material. The BCB is spin-coated and baked in multiple stages to achieve a smooth and uniform profile. This process is repeated five times to achieve a total BCB thickness of about 25 µm. Following the spin and bake steps, the top surface of the BCB is etched using reactive ion etching (RIE) to the same height of the active region waveguides, ensuring a flat, continuous surface across the entire device. Subsequently, an extended top metallization is deposited over the active region and the BCB-covered area on the sides, completing the fabrication of the laser chip with well-defined waveguides and metal structures.

The fabricated samples were then cleaved into smaller chips and mounted onto a copper submount with a custom RF-optimized PCB by die bonding with indium paste and wire bonding for the electrical connections. The PCB is a crucial component for efficient microwave modulation. The bonded chip was then mounted on a cryostat cold finger. Electrical connections are made accessible from the outside of the cryostat using a standard RF connector (HK-LR-SR2) and low-loss semi-rigid RF cables (SUCOFORM 86 FEP).

Simulation and design

The device optimization was carried out with SPINS [2]. The mesh grid size and the minimum feature size (related to fabrication constraints) were both set to 4 µm. The allowed permittivity values for the final design were set to the active region (n_{GaAs}=3.6, dispersive) and the BCB (n_{BCB}=1.6, constant). The software runs a gradient-based topology optimization, by computing the value and the gradient of a given figure of merit (the objective function) and modifying the topology to minimize it. To produce highly performing devices, the software performs some transformations that change the parametrization of the permittivity distribution from discrete to continuous and viceversa. The final design must obey to the fabrication constraints initially set,

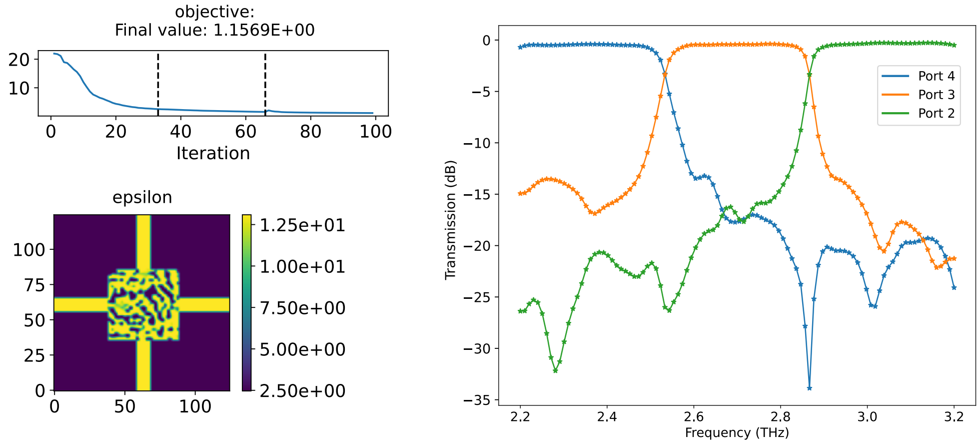

Figure S1: Outcome of the WDM optimization carried out with SPINS. On the left, the convergence to a minimum value of the objective function and the corresponding final permittivity distribution. On the right the simulated transmission.

therefore a discretization operation that optimizes the discrete final design is performed last. For the device presented in this work, the objective function was defined as the sum of 21 identical sub-objectives (7 per channel), one for each optimization frequency. The sub-objective was defined as the difference between the target transmission (T=1) and the simulated transmission at the wanted output. After 105 iterations the method converged to a final design with the best figure of merit (see Fig.S1). The running time for a single optimization is less than two hours.

To validate the results of the optimization and investigate the final device design with the two active sections with a passive junction, a full 3D broadband time-domain numerical simulation of the structure is performed with CST Studio Suite. As displayed in Fig.S2, the overall performance is confirmed, although with higher losses and cross-talk compared to the SPINS simulation (where only the WDM section was simulated). The additional losses

Experimental Methods

For all the measurements, the device was mounted on a cold finger cryostat and cooled down to an operating temperature of 20 K by using a liquid helium transfer line and stabilizing the heat

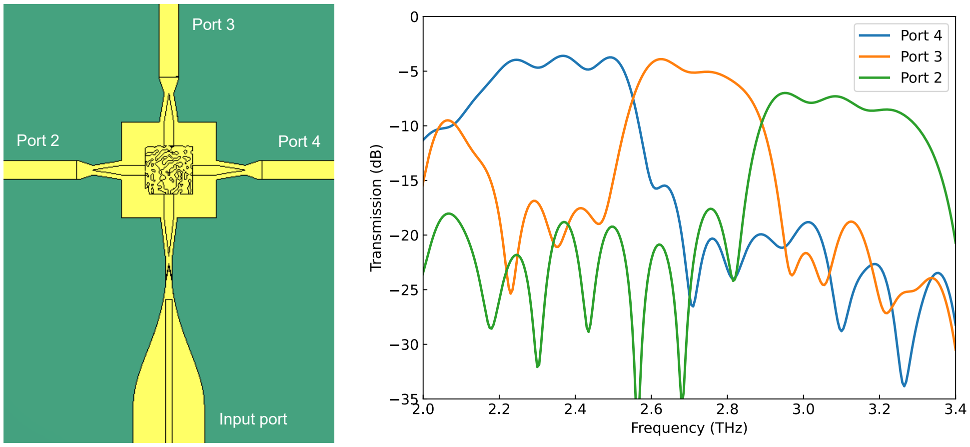

Figure S2: Overview of the CST 3D broadband time-domain simulation. On the left, the simulated structure with the input coming from the QCL section, the coupling to the WDM section through the passive transition, and the collection of the output from the passive waveguides in correspondance of each output port of the WDM. In the real device, the passive waveguides are replaced by the surface-emitting antennas. On the right the simulated transmission.

sink temperature with a temperature controller.

The laser was operated in continuous-wave mode, using a Keithley 2420 source, or in pulsed mode with an Agilent 8114A pulse generator. Additional microwave modulation was supplied using a Rohde&Schwarz SMB 100A microwave signal generator in combination with a Mini-Circuits ZVE-3W-183+ microwave amplifier.

The laser emission spectra were obtained using a Bruker Vertex 80v, a Fourier transform infrared spectrometer (FTIR) with a room-temperature deuterated triglycine sulfate (DTGS) detector. The optics and sample compartments of the FTIR were evacuated to avoid any THz absorption.

For SWIFT spectroscopy measurements [3], a Schottky diode [4] was used as a fast detector at room temperature. The beatnote signal was collected at the FTIR output and measured with a Rohde&Schwarz FSW67 RF spectrum analyzer with an IQ demodulator function. A detailed description of the experimental setup can be found in Ref. [1].

Additional Results

In the following, we present additional experimental results on the same planarized THz QCL device with the integrated inverse-designed WDM presented in the main manuscript.

Free-running beatnote maps

In Fig. S3, we show the results of the measurements of the electrical beatnote of the THz QCL comb obtained sweeping the bias voltage of the laser and for different values of the voltage applied to the WDM section. The QCL shows a stable RF beatnote at the fundamental (15.65 GHz) and its harmonics $2f_{rep}$ and $3f_{rep}$, regardless of the operating point of the WDM section. It follows that the feedback in the laser cavity introduced by the latter is weak enough to keep the free-running comb operation of the QCL stable, apart from some instability arising for laser voltages below 8 V.

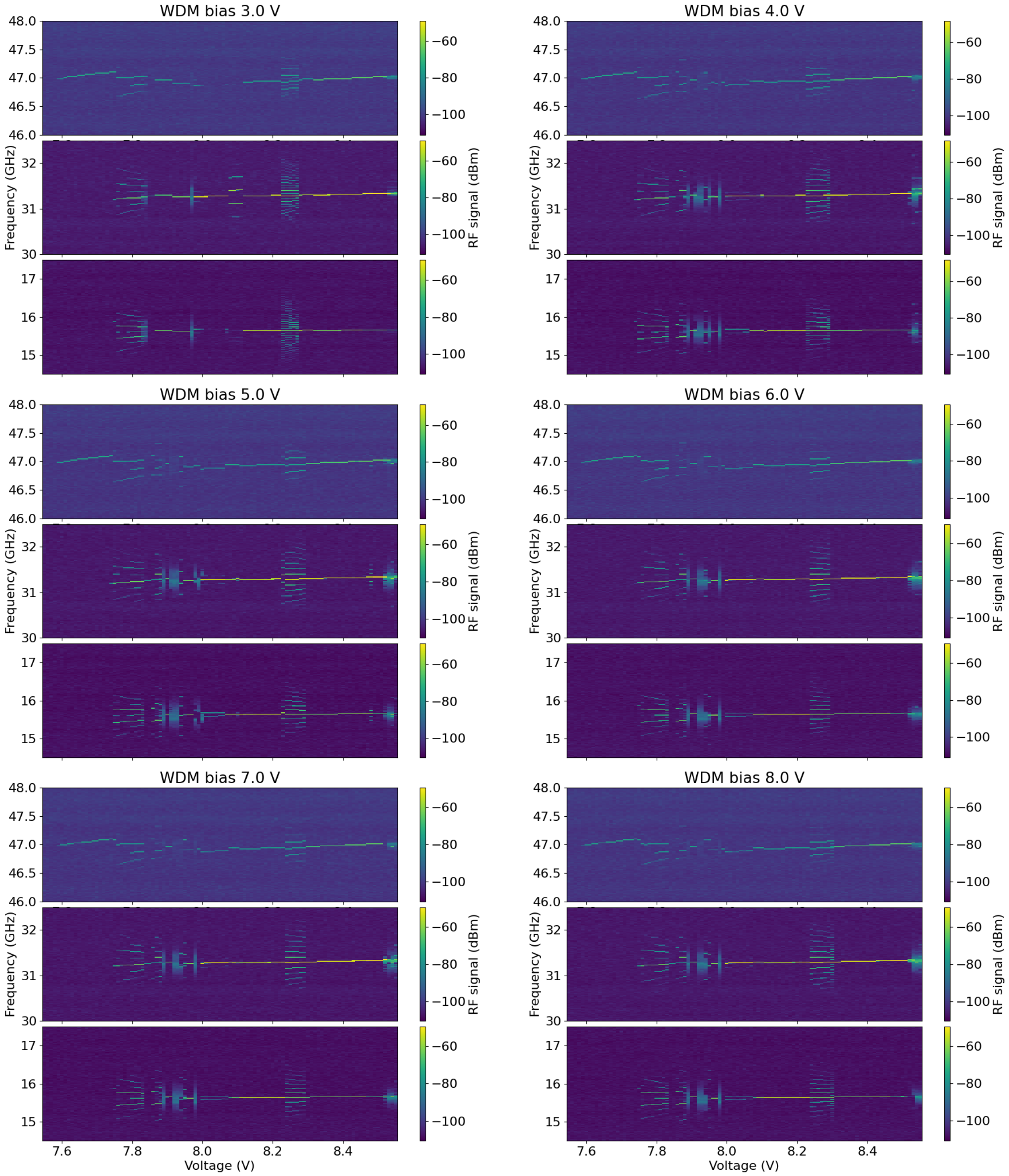

Figure S3: Detailed results of the free-running electrical beatnote of the QCL obtained for different applied voltages to the WDM section, sweeping the bias of the laser. These maps show the absence of any significant feedback coming from the WDM section, which does not affect the operation of the QCL as a frequency comb source.

References

[1] Urban Senica et al. “Planarized THz quantum cascade lasers for broadband coherent photonics”. In: *Light: Science & Applications* 11.347 (2022).

[2] Logan Su et al. “Nanophotonic inverse design with SPINS: Software architecture and practical considerations”. In: *Applied Physics Reviews* 7.1 (2020), p. 011407.

[3] David Burghoff et al. “Evaluating the coherence and time-domain profile of quantum cascade laser frequency combs”. In: *Optics express* 23.2 (2015), pp. 1190–1202.

[4] V.G. Bozhkov. “Semiconductor Detectors, Mixers, and Frequency Multipliers for the Terahertz Band”. In: *Radiophysics and Quantum Electronics* 46 (2003), pp. 631–656.